Available online at www.sciencedirect.com

ScienceDirect

Ceramics International 40 (2014) 707–713

CERAMICS INTERNATIONAL

www.elsevier.com/locate/ceramint

Phase composition, microstructure and mechanical properties of ZrC coatings produced by chemical vapor deposition

Ying Long[a,b,*], Athar Javed[c], Jie Chen[b], Zhao-ke Chen[b], Xiang Xiong[b]

[a]School of Electromechanical Engineering, Guangdong University of Technology, Guangzhou Higher Education Mega Center, No. 100 Waihuan Xi Road, Panyu District, Guangzhou 510006, PR China

[b]State Key Laboratory for Powder Metallurgy, Central South University, Changsha 410083, PR China

[c]Department of Physics, University of the Punjab, Quaid-i-Azam Campus, Lahore-54590, Pakistan

Received 29 April 2013; received in revised form 17 June 2013; accepted 17 June 2013
Available online 2 July 2013

Abstract

We report results on stoichiometric and non-stoichiometric ZrC coatings produced on graphite substrates by chemical vapor deposition (CVD) in the $ZrCl_4$–CH_4–Ar system. The phase composition, microstructure and mechanical properties of both (ZrC and $ZrC_{0.85}$) coatings were studied. X-ray diffraction (XRD) confirmed the formation of cubic ZrC. A strong (200) texture normal to the substrate surface was observed in both coatings which were confirmed by scanning electron microscopy (SEM). X-ray photoelectron spectroscopy (XPS) showed ZrC to be the main phase in both coatings with ~5.5 mol% ZrO_2 minor phase. In stoichiometric ZrC coating, both Young's modulus (312 ± 9 GPa) and hardness (25 ± 3.1 GPa) were higher compared to the non-stoichiometric $ZrC_{0.85}$ coating.

Keywords: C. Mechanical properties; Stoichiometry; Phase composition; ZrC coating

1. Introduction

Zirconium carbide (ZrC) is one of the well-known refractory metal carbides, which has unique combination of chemical, structural and mechanical properties. For example, ZrC has high melting point (~3540 °C), high thermal conductivity, good chemical stability and excellent mechanical properties at an elevated temperature [1–3]. Due to an excellent combination of structural compatibility and mechanical properties, ZrC is a promising hard ceramic material for a wide range of applications which includes its use in machining tools, hard-coating industry and electronic devices [4–9]. ZrC also has potential applications as coating material for nuclear fuel in future generation IV nuclear reactors due to its high resistance to corrosion by fission products [2,4–9]. Deposition techniques such as dc magnetron sputtering [10], chemical vapor deposition (CVD) [11] and pulsed laser deposition (PLD) [12–16] have been adopted to grow high quality, dense and defect free ceramic coatings. Among these deposition methods, CVD is widely used to deposit high quality ceramic coatings [11,17,18]. Further, it has been demonstrated that the use of zirconium tetrachloride ($ZrCl_4$) as source material for zirconium offers a tight and relatively easy control on the flow of $ZrCl_4$ vapors when enters into the CVD furnace during CVD process [11]. Through CVD, various groups [19–24] have successfully produced near theoretical density and oxide-free condensates of hard ceramic coatings. However, in hard ceramic coatings (such as SiC and ZrC) produced by CVD, the phase composition, microstructure and mechanical properties are greatly affected by the chosen combination of deposition parameters [3,9,25–27].

It is known from literature that the deposition parameters (in CVD) such as gas-flow rate, molar ratio of different species, deposition temperature and substrate position have significant effects on microstructure and mechanical properties of such coatings [5,28,29]. ZrC crystallizes in B1 (NaCl)-type lattice and can exhibit a wide range of zirconium (Zr) to carbon (C) ratio [2]. From the phase diagram of Zr–C system (see Fig. 4 in

*Corresponding author at: Guangdong University of Technology, School of Electromechanical Engineering, Guangzhou Higher Education Mega Center, No. 100 Waihuan Xi Road, Guangzhou 510006, China.
Tel.: +0086 155 2113 9315; fax: +0086 020 3932 2925.
E-mail addresses: longying0306@gmail.com (Y. Long), xiong228@sina.com (X. Xiong).

0272-8842/$ - see front matter © 2013 Elsevier Ltd and Techna Group S.r.l. All rights reserved.
http://dx.doi.org/10.1016/j.ceramint.2013.06.059

Ref. [4]) it is known that the ZrC phase exists when the molar ratio of carbon to zirconium is in the range of 0.61:1–1:1 at 500 °C [4,6]. During growth of ZrC coating by CVD, a non-stoichiometric ZrC could be formed having some concentration of carbon vacancies. Non-stoichiometry may deteriorate the mechanical properties as compared to the stoichiometric ZrC coating [4]. Thus, it is worth studying how the structure and mechanical properties of non-stoichiometric ZrC coating differ from stoichiometric coating [30]. So far, very few papers have been published on studying the mechanical properties of ZrC coating and according to our knowledge, work is not reported on comparing the properties of stoichiometric and non-stoichiometric ZrC coatings produced by CVD.

In the present study, we have produced two sets of ZrC coating by CVD with different Zr to C ratio (i.e. stoichiometric ZrC and non-stoichiometric $ZrC_{0.85}$) and studied their phase composition, microstructure, surface chemistry and mechanical properties. Phase composition and microstructure were studied using standard techniques such as X-ray diffraction (XRD) and scanning electron microscopy (SEM). Surface chemistry of both coatings was analyzed by applying a surface sensitive technique such as X-ray photoelectron spectroscopy (XPS). A correlation between phase composition, microstructure and mechanical properties of both stoichiometric and non-stoichiometric ZrC coatings is developed and discussed here.

2. Experiments details

2.1. Sample preparation

Zirconium carbide (ZrC) coatings were produced on graphite substrates by CVD at a temperature of 1550 ± 5 °C. Fig. 1 shows the schematic diagram of CVD system used for the growth of ZrC coatings. High purity graphite substrates (size $30 \times 20 \times 5$ cm^3) were placed in the hot zone of CVD reactor (see Fig. 1) and coating was allowed to grow for 3 h. Before deposition, the substrates were cleaned ultrasonically in acetone followed by cleaning with ethanol. After substrates cleaning, the substrates were placed on the substrate table in the CVD reactor (see Fig. 1). For ZrC coating, zirconium tetrachloride ($ZrCl_4$) powder (purity 99.9%) and high purity methane (CH_4) were used as source materials for Zr and C, respectively. Purified hydrogen (H_2) gas was used as a reducing agent for $ZrCl_4$ vapor and argon (Ar) gas was used as a carrier gas for $ZrCl_4$ and also as a dilution gas. Two different sets of coatings (i.e. stoichiometric ZrC and non-stoichiometric $ZrC_{0.85}$) were obtained by placing graphite substrates at positions marked in the CVD reactor (see Fig. 1). The summary of the deposition parameters used to produce ZrC coatings are listed in Table 1. In the CVD reactor, ZrC coatings are formed as a result of the following chemical reactions:

$$ZrCl_4 + H_2 \rightarrow ZrCl_x + HCl \ (x = 0, 1, 2, 3) \quad (1)$$

$$CH_4 \rightarrow C + H_2 \quad (2)$$

$$ZrCl_x + C \rightarrow ZrC + xCl \quad (3)$$

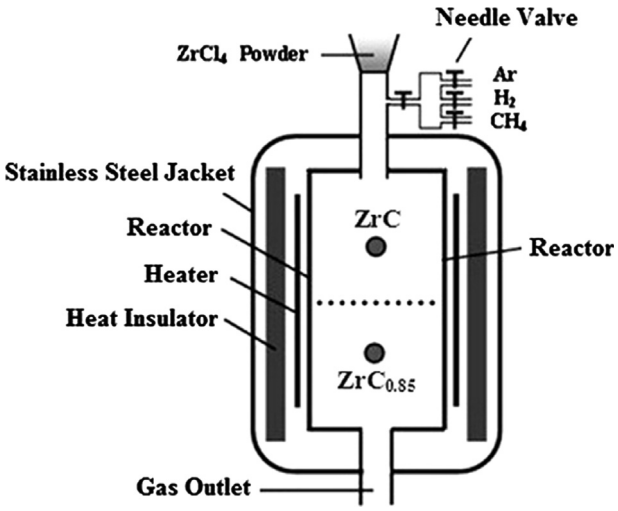

Fig. 1. Schematic diagram of the CVD system used to produce ZrC coatings. In the CVD reactor, the substrate positions are marked as solid spheres (•) giving stoichiometric ZrC and non-stoichiometric $ZrC_{0.85}$ coatings.

Table 1
Summary of deposition parameters for ZrC coatings produced by CVD.

Deposition temperature (°C)	Deposition pressure (Pa)	Gas flow rate (ml min^{-1})			Deposition time (h)
		H_2	Ar	CH_4	
1550 ± 5	5000 ± 50	900	800	100	3

$$Cl + H_2 \rightarrow HCl \quad (4)$$

2.2. Characterization

The surface morphology and microstructure of both coatings were studied by field-emission scanning electron microscopy (SEM, FE-SEM Philips XL30 FEG, The Netherlands). Both surface and cross-sectional SEM images were taken for all samples to elucidate the microstructure and growth features. X-ray diffraction (Philips PW-1830 X-ray diffractometer, The Netherlands) with Cu K_α radiation and operated at 40 kV and 25 mA was used to study the phase composition. X-ray photoelectron spectroscopy (XPS) [Thermo Fisher Scientific K-Alpha 1063 spectrometer with a monochromatic Al-K_α (1486.6 eV) X-ray source] was used to study the surface compositions/stoichiometry of coatings. XPS spectra were recorded (in the range of 0–1400 eV) for both samples. XPS spectra were collected at 50 eV constant pass energy while high resolution XPS spectra of Zr 3d and C 1s core-levels were taken at 20 eV pass energy. XPS spectra were processed using thermal advantage 4.75 analysis software, which allows smoothing and de-convolution of curves. The hardness (H) and Young's modulus (Y) of ZrC coatings were measured with a commercially available micro-indentation device (CSM) equipped with a Vickers indenter. At least 10 indentations

per sample were made and the data were averaged over all measurements to calculate H and Y for both coatings. The indentation experiment was performed in load control mode with a load maximum up to 300 mN. This ensures the exclusion of substrate contribution in the measurements. Both hardness (H) and Young's modulus (Y) were determined from the load-displacement micro-indentation data by following the method purposed by Olive and Pharr [31].

3. Results and discussion

3.1. Microstructure and phase composition analysis

Fig. 2 shows the SEM images of ZrC coatings. From Fig. 2(a) it can be seen that the as-deposited ZrC coating exhibits a wavy structure without any obvious crack on the coating surface. However, high magnification SEM image (Fig. 2(b)) shows the agglomeration of equal sized grains of spherical shape. Similar surface morphology of ZrC coatings grown on C/C composites has been observed by Wang et al. [32]. The SEM image (Fig. 2(c)) taken from the cross-section of the ZrC coating shows that the coating has a columnar growth structure with thickness 100 ± 2 μm. The coating shows a good adhesion with the substrate. Comparing the SEM images of both coatings, no significant difference between surface morphology and microstructure were observed in both coatings. Further, high magnification cross-sectional SEM image (Fig. 2(d)) reflects a highly dense coating.

Fig. 3 shows the XRD patterns of as-deposited ZrC coatings. XRD spectra showed that the both coatings exhibited a crystalline structure with a strong (200) texture normal to the substrate surface. Comparing the XRD spectra of both samples, it was observed that the peak position corresponding to the (200) reflection in non-stoichiometric $ZrC_{0.85}$ coating shifted slightly towards the lower 2θ value compared to the stoichiometric ZrC coating (see Fig. 3b). This peak shift (towards lower 2θ value) in non-stoichiometric ZrC coating is found consistent with the findings of Wang et al. [4].

The lattice parameters of both coatings ($ZrC_{0.85}$ and ZrC) were calculated and are listed in Table 2. It was found that the lattice parameter of stoichiometric ZrC coating was 4.693 Å, which was slightly larger than that of non-stoichiometric $ZrC_{0.85}$ coating (see Table 2). This is in agreement with the results reported by Nachiappan et al. [33] and Wang et al. [4]. They also found a slight decrease in the lattice parameter for non-stoichiometric ZrC_x with the decrease in carbon content. This can be attributed to the presence of more carbon vacancies in ZrC_x ($x=0$–1) with the decrease in x.

Fig. 4 shows the XPS survey spectrum of ZrC coating. The main peaks observed and the corresponding phases are indicated on the XPS spectrum. The analysis of XPS spectra of both samples confirmed the presence of Zr and C atoms as

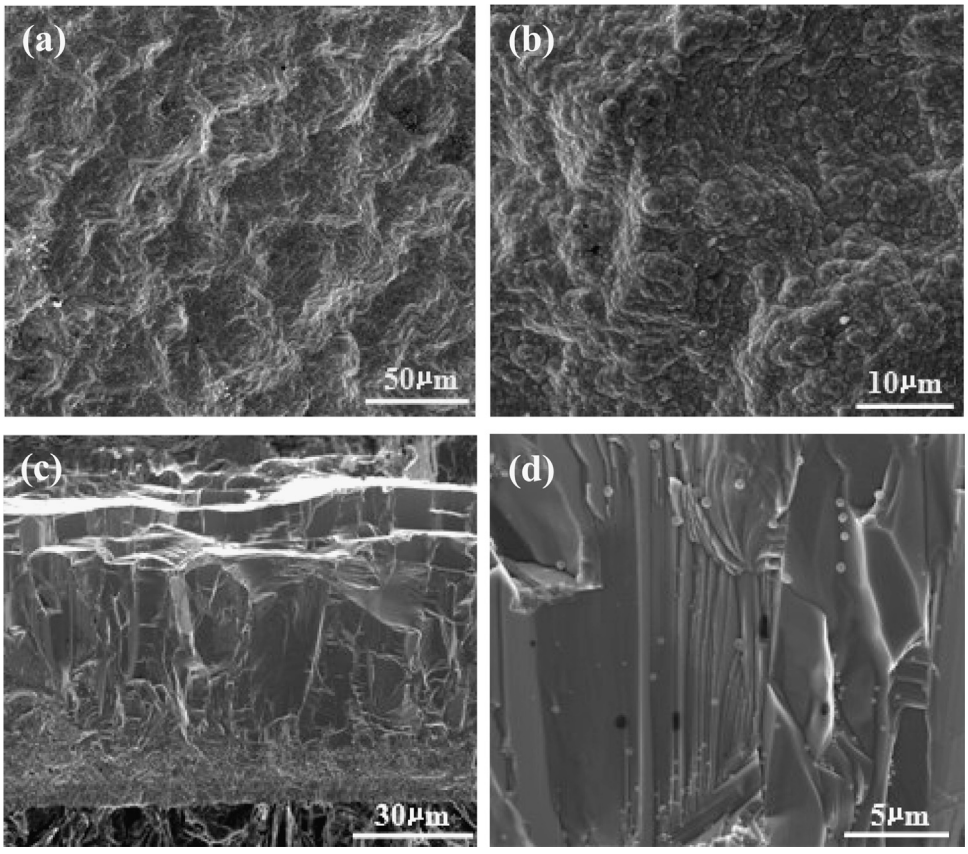

Fig. 2. SEM images of ZrC coating (a–b) surface SEM images showing the surface morphology (c–d) cross-sectional SEM images showing the columnar growth structure.

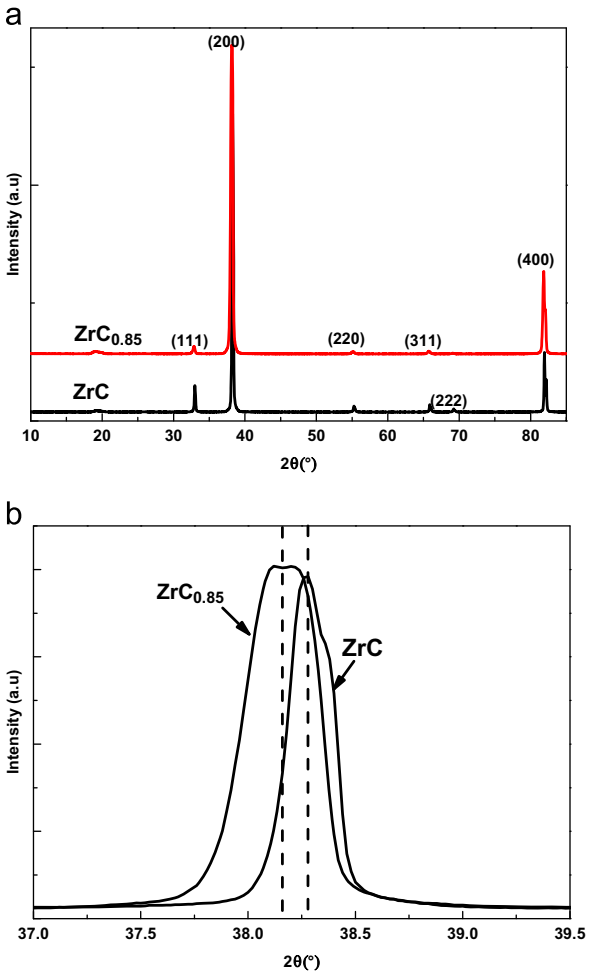

Fig. 3. (a) XRD patterns of ZrC and $ZrC_{0.85}$ coatings and (b) expanded XRD (200) peak for both spectra showing the shift in peak.

Table 2
Lattice parameter (calculated using XRD results) of ZrC and $ZrC_{0.85}$ coatings.

Sample	JCPDS #	Lattice parameter (Å)
ZrC	35–0784	4.693
$ZrC_{0.85}$	65–8836	4.692

surface elements. However, the peaks corresponding to the oxygen (O) were also observed. This meant that the surface of the coating was contaminated by oxygen to some extent and resulted in the formation Zr–O bond [34].

Zr 3d and C 1 s core-level spectra of ZrC and $ZrC_{0.85}$ coatings are presented in Fig. 5(a) and (b). From the analysis of XPS spectra, it was found that the binding energy for ZrC and $ZrC_{0.85}$ coating corresponding to Zr 3d peak decreased. However, in both coatings the carbide (C 1s) peak appears at the same value of the binding energy. This is consistent with the change in stoichiometry of Zr and C in ZrC [34,35]. Fig. 6 shows the schematic explaining the atomic sites of Zr and C atoms in stoichiometric and non-stoichiometric ZrC system.

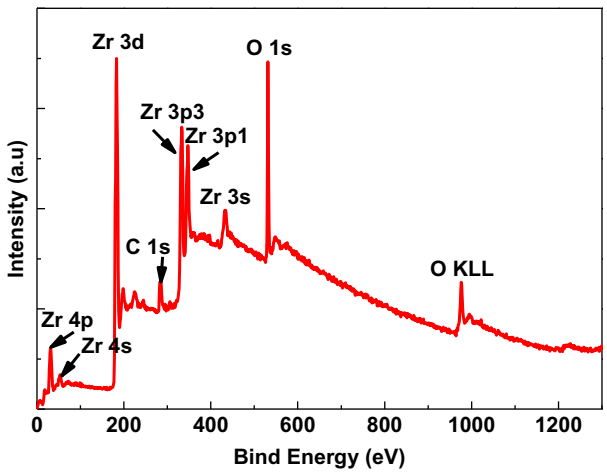

Fig. 4. XPS survey spectrum of ZrC coating showing the peaks appearing from different energy levels.

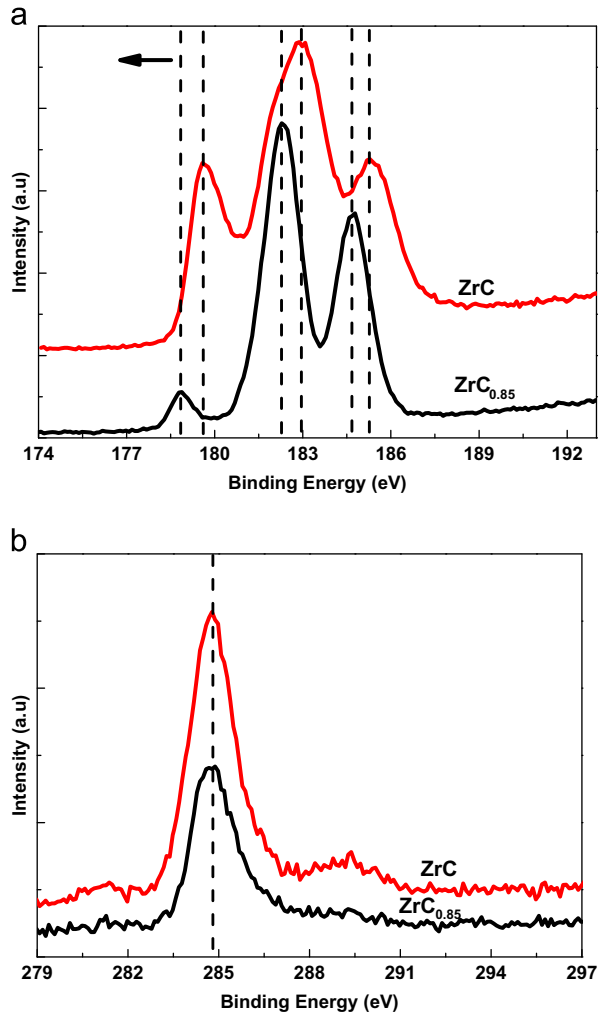

Fig. 5. XPS spectra showing the intensity variation at the core-levels in stoichiometric ZrC and non-stoichiometric $ZrC_{0.85}$ coatings corresponding to (a) Zr 3d and (b) C 1s energy levels.

As C/Zr ratio increases from non-stoichiometry (carbon content = 0.85) towards stoichiometry, the nearest neighbor environment of C atoms within ZrC remains almost unchanged, but

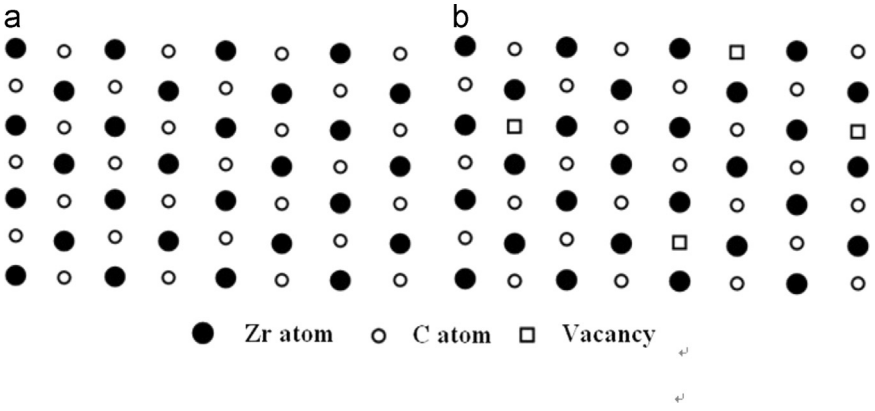

Fig. 6. Schematic diagram showing the sites of Zr and C atoms in (a) stoichiometric ZrC system and (b) non-stoichiometric i.e. ZrC_x ($x < 1$) system.

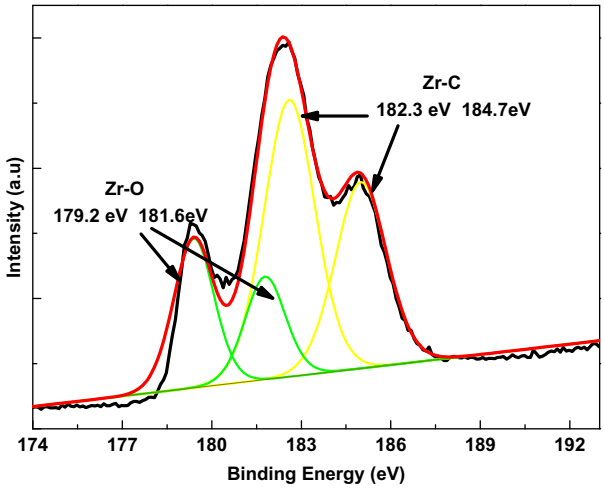

Fig. 7. High resolution XPS spectrum of ZrC coating. Fitting curves are shown with their binding energies relative to the Zr 3d band.

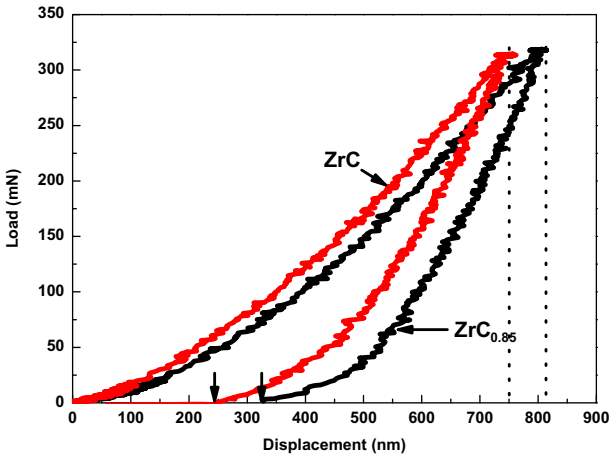

Fig. 8. Representative load-displacement curves for stoichiometric ZrC and non-stoichiometric $ZrC_{0.85}$ coatings. The data was taken with a maximum given load of 300 mN.

for the Zr atoms there is an increase in the nearest neighbor C atoms, therefore the Zr 3d peaks shift towards the higher binding energy side (see Figs. 5 and 6).

Fig. 7 shows the high-resolution XPS spectra with fitting curves relative to the Zr 3d band. The peak corresponding to the Zr 3d band is composed of spin–orbit doublets (i.e. Zr $3d_{5/2}$ and Zr $3d_{3/2}$) each separated by energy difference, $\Delta E = 2.4$ eV. Deconvolution of the Zr 3d peak showed that the binding energies of Zr atoms involved are 179.2 eV, 181.6 eV, 182.3 eV and 184.7 eV. The binding energies of 182.3 eV and 184.7 eV correspond to the Zr–C bond while the binding energies of 179.2 eV and 181.6 eV correspond to the Zr–O bond [24,35]. The ratio of these two kinds of bonds (i.e. Zr–C and Zr–O bond) is 88.9% and 11.1%, respectively. This indicates the presence of ~5.5 mol% ZrO_2 minor phase in the ZrC coating. The appearance of ZrO_2 minor phase can be attributed to the high affinity between Zr and O during and/or after coating [9,35]. As the content of ZrO_2 minor phase (measured by XPS in the ZrC coating) is only about 5.5 mol%, therefore, it is reasonably acceptable that the oxygen (O) containing phase of Zr can be detected by a surface sensitive technique such as XPS which was not possible to detect by XRD [24].

3.2. Hardness and Young's modulus

Fig. 8 shows the representative micro-indentation load–displacement curves for stoichiometric and non-stoichiometric ZrC coatings. It can be seen that with a given load of 300 mN, the displacement in the non-stoichiometric $ZrC_{0.85}$ coating is ~820 nm, which is larger than that observed in stoichiometric ZrC coating (~750 nm). This means that the mechanical properties (i.e. hardness, H and Young's modulus, Y) of non-stoichiometric $ZrC_{0.85}$ coating are lower when compared with the stoichiometric ZrC coating. The hardness and Young's modulus of both coatings were calculated from the load–displacement curves by following the method purposed by Olive and Pharr [31]. The calculated hardness and Young's modulus data are listed in Table 3. Comparing the mechanical properties of both coatings, it was found that the hardness of

Table 3
Vickers hardness (H) and reduced Young's modulus (Y) of stoichiometric ZrC and non-stoichiometric $ZrC_{0.85}$ coatings.

Sample	Hardness (H) (GPa)	Young's modulus (Y) (GPa)
ZrC	25.3 ± 1.3	312 ± 9
$ZrC_{0.85}$	22.8 ± 1.3	302 ± 11

stoichiometric ZrC coating was 3 GPa higher compared to the non-stoichiometric $ZrC_{0.85}$ coating while the stoichiometric ZrC coating has Young's modulus 11 GPa higher than that of non-stoichiometric $ZrC_{0.85}$ coating. As discussed above, the surface morphology, microstructure and texture of both (ZrC and $ZrC_{0.85}$) coatings are more or less similar, thus it appears that the difference in phase composition determines the mechanical properties in the coatings studied here. Polychronopoulou et al. [36] studied the hardness and Young's modulus of TiC_x ($x=0$–1) coatings and found an increase in both hardness and Young's modulus with the increase in carbon content. As both zirconium and titanium belong to the same group, therefore similarity in mechanical properties may exist. The decrease in mechanical properties can be attributed to the density of carbon (C) vacancies as the density of C atoms decreases in the ZrC_x lattice when carbon content, x decreases from $x=1$ to $x=0$.

4. Conclusions

In conclusion, the stoichiometric and non-stoichiometric ZrC coatings were produced on graphite substrates by CVD. The phase composition, microstructure and mechanical properties were studied by X-ray diffraction (XRD), scanning electron microscope (SEM), X-ray photoelectron spectroscopy (XPS) and micro-indentation techniques. The results showed that the ZrC coatings exhibited a crystalline cubic structure with strong (200) texture normal to the substrate surface. XPS spectra confirmed ZrC to be the main phase in both coatings with ~5.5 mol% ZrO_2 minor phase. XPS spectra of Zr 3d band shift towards the lower binding energy (for non-stoichiometric $ZrC_{0.85}$) while the C 1s peak appears at the same value of the binding energy in both coatings. Both hardness and Young's modulus of non-stoichiometric $ZrC_{0.85}$ coating were lower compared to the stoichiometric ZrC coating.

Acknowledgment

This research work was supported by the Natural Science Foundation of Hunan Province of China through Project no. 12JJ6051. One of the authors (A. Javed) is thankful to Paul Hawksworth (who is with Department of Materials Science and Engineering, University of Sheffield, UK) for his support in proof reading this manuscript to improve English.

References

[1] J. Xie, K. Li, H. Li, Q. Fu, L. Guo, Ablation behavior and mechanism of C/C–ZrC–SiC composites under an oxyacetylene torch at 3000 °C, Ceramics International 39 (2013) 4171–4178.
[2] V. Craciun, D. Craciun, J.M. Howard, J. Woo, Pulsed laser deposition of crystalline ZrC thin films, Thin Solid Films 515 (2007) 4636–4639.
[3] J.H. Park, C.H. Jung, D.J. Kim, J.Y. Park, Temperature dependency of the LPCVD growth of ZrC with the $ZrCl_4$–CH_4–H_2 system, Surface and Coatings Technology 203 (2008) 324–328.
[4] X.-G. Wang, W.-M. Guo, Y.-M. Kan, G.-J. Zhang, P.-L. Wang, Desification behavior and properties of hot-pressed ZrC ceramics with Zr and graphite additives, Journal of the European Ceramic Society 31 (2011) 1103–1111.
[5] J.H. Park, C.H. Jung, D.J. Kim, J.Y. Park, Effect of H_2 dilution gas on the growth of ZrC during low pressure chemical vapor deposition in the $ZrCl_4$–CH_4–Ar system, Surface and Coatings Technology 203 (2008) 87–90.
[6] Y.S. Won, W.G. Varanasi, O. Kryliouk, T.J. Anderson, L.M. White, R.J. Perez, Equilibrium analysis of zirconium carbide CVD growth, Journal of Crystal Growth 307 (2007) 302–308.
[7] S. Xuetao, L. Kezhi, L. Hejun, D. Hongying, C. Weifeng, L. Fengtao, Microstructure and ablation properties of zirconium carbide doped carbon/carbon composites, Carbon 48 (2010) 344–351.
[8] W. Sun, X. Xiong, B.Y. Huang, G.D. Li, H.B. Zhang, P. Xiao, Z.K. Chen, X.L. Zheng, Preparation of ZrC nano-particles reinforced amorphous carbon composite coating by atmospheric pressure chemical vapor deposition, Applied Surface Science 255 (2009) 7142–7146.
[9] B. Liu, C. Liu, Y. Shao, J. Zhu, B. Yang, C. Tang, Deposition of ZrC-coated particle for HTR with $ZrCl_4$ powder, Nulcear Engineering and Design 251 (2012) 349–353.
[10] M. Andersson, S. Urbonaite, E. Lewin, U. Jansson, Magnetron sputtering of Zr–Si–C thin films, Thin Solid Films 520 (2012) 6375–6381.
[11] H. Zhao, B. Liu, K. Zhang, C. Tang, Microstructure analysis of zirconium carbide layer on pyrocarbon-coated particles prepared by zirconium chloride vapor method, Nuclear Engineering and Design 251 (2012) 443–438.
[12] L. D' Alessio, A. Santagata, R. Teghil, M. Zaccagnino, I. Zacardo, V. Marotta, D. Ferroc, G. De Maria, Zirconium carbide thin films deposited by pulsed laser ablation, Applied Surface Science 168 (2000) 284–287.
[13] V. Craciun, J. Woo, D. Craciun, R.K. Singh, Epitaxial ZrC thin films grown by pulsed laser deposition, Applied Surface Science 252 (2006) 4615–4618.
[14] D. Craciun, G. Socol, G. Dorcioman, N. Stefan, G. Bourne, V. Craciun, High quality ZrC, ZrC/ZrN and ZrC/TiN thin films grown by pulsed laser deposition, Journal of Optoelectronics and Advanced Materials 12 (2010) 461–465.
[15] D. Craciun, G. Bourne, J. Zhang, K. Siebein, G. Socol, G. Dorcioman, V. Craciun, Thin and hard ZrC/TiN multilayers grown by pulsed laser deposition, Surface and Coating Technology 205 (2011) 5493–5496.
[16] V. Craciun, E.J. McCumiskey, M. Hanna, C.R. Taylor, Very hard ZrC thin films grown by pulsed laser deposition, Journal of the European Ceramic Society 33 (2013) 2223–2226.
[17] Z. Chen, S. Li, Z. Liu, Morphology and growth mechanism of CVD alumina–silica, Ceramics International 31 (2005) 1103–1107.
[18] Z.F. Chen, Aluminosilicate coating prepared by low pressure chemical vapor deposition using TEOS and $AlCl_3$ as precursors, Surface Engineering 26 (2010) 607–609.
[19] Z.-K. Chen, X. Xiong, Y. Long, Influence of $TaCl_5$ partial pressure on texture structure of TaC coating deposited by chemical vapor deposition, Applied Surface Science 257 (2010) 4044–4050.
[20] G. Li, S. Chakrabarti, M. Schulz, V. Shanov, The effect of substrate positions in chemical vapor deposition reactor on the growth of carbon nanotube arrays, Carbon 48 (2010) 2111–2115.
[21] D.C. Johnson, W.D. Morris, A.L. Prieto, Effects of transport gradients in a chemical vapor deposition reactor employing vapor–liquid–solid growth of ternary chalcogenide phase-change materials, Nanotechnology 21 (2010) 165604.

[22] X. Xiong, Z.-K. Chen, B.-Y. Huang, G.-D. Li, F. Zheng, P. Xiao, H.-B. Zhang, Surface morphology and preferential orientation growth of TaC crystals formed by chemical vapor deposition, Thin Solid Films 517 (2009) 3235–3239.
[23] K.-I. Park, J.-H. Kim, H.-K. Lee, D.K. Kim, High temperature mechanical properties of CVD-SiC thin films, Modern Physics Letters B 23 (2009) 3877–3886.
[24] Y.S. Won, Y.S. Kim, V.G. Varanasi, O. Kryliouk, T.J. Anderson, C.T. Sirimanne, L.M. White, Growth of ZrC thin films by aerosol-assisted MOCVD, Journal of Crystal Growth 304 (2007) 324–332.
[25] C. Lu, L. Cheng, C. Zhao, L. Zhang, Y. Xu, Kinetics of chemical vapor deposition of SiC from methyltrichlorosilane and hydroden, Applied Surface Science 255 (2009) 7495–7499.
[26] H.-S. Kim, D.-J. Choi, Effect of diluent gases on growth behavior and characteristics of chemically vapor deposited silicon carbide films, Journal of the American Ceramic Society 82 (1999) 331–337.
[27] B.J. Choi, D.R. Kim, Growth of silicon carbide by chemical vapour deposition, Journal of Materials Science Letters 10 (1991) 860–862.
[28] Y. Long, A. Javed, I. Shapiro, Z.-K. Chen, X. Xiong, P. Xiao, The effect of substrate position on the microstructure and mechanical properties of SiC coatings on carbon/carbon composites, Surface and Coatings Technology 206 (2011) 568–574.
[29] Y. Yang, W.G. Zhang, Chemical vapor deposition of SiC at different moral ratios of hydrogen to methyltrichlorosilane, Journal of Central South University of Technology 16 (2009) 730–737.
[30] Y. Xu, L. Cheng, L. Zhang, W. Zhou, Morphology and growth mechanism of silicon carbide chemical vapor deposited at low temperatures and normal atmosphere, Journal of Materials Science 34 (1999) 551–555.
[31] W.C. Oliver, G.M. Pharr, Measurement of hardness and elastic modulus by instrumented indentation: advances in understanding and refinements to methodology, Journal of Materials Research 19 (2004) 3–20.
[32] S.-L. Wang, K.-Z. Li, H.-J. Li, Y.-L. Zhang, Microstructure and ablation resistance of ZrC nanostructured coating for carbon/carbon composites, Materials Letters 107 (2013) 99–102.
[33] C. Nachiappan, L. Rangaraj, C. Divakar, V. Jayaram, Synthesis and densification of monolithic zirconium carbide by reactive hot pressing, Journal of the American Ceramic Society 93 (2010) 1341–1346.
[34] M. Balaceanu, M. Braic, V. Braic, A. Vladescu, C.C. Negrila, Surface chemistry of plasma deposited ZrC hard coatings, Journal of Optoelectronics and Advanced Materials 7 (2005) 2557–2560.
[35] C.L. Chu, H.L. Ji, L.H. Yin, Y.P. Pu, P.H. Lin, P.K. Chu, Fabrication, properties, and cytocompatibility of ZrC film on electropolished NiTi shape memory alloy, Materials Science and Engineering C 31 (2011) 423–427.
[36] K. Polychronopoulou, C. Rebholz, M.A. Baker, L. Theodorou, N. G. Demas, S.J. Hinder, A.A. Polycarpou, C.C. Doumanidis, K. Böbel, Nanostructure, mechnical and tribological properties of reactive magnetron sputtered TiC_x coatings, Diamond and Related Materials 17 (2008) 2054–2061.